Journal of ELECTRONIC MATERIALS, Vol. 47, No. 9, 2018
https://doi.org/10.1007/s11664-018-6398-z

Thermal, Structural, AC Conductivity, and Dielectric Properties of Ethyl-2-amino-6-ethyl-5-oxo-4-(3-phenoxyphenyl)-5,6-dihydro-4*H*-pyrano[3,2-*c*]quinoline-3-carboxylate Thin Films

M.M. EL-SHABAAN[1,2]

1.—Department of Physics, Faculty of Science, Damietta University, Damietta 34517, Egypt.
2.—e-mail: elshabaan@gmail.com

Thermal, structural, alternating-current (AC) conductivity (σ_{AC}), and dielectric properties of ethyl-2-amino-6-ethyl-5-oxo-4-(3-phenoxyphenyl)-5,6-dihydro-4*H*-pyrano[3,2-*c*]quinoline-3-carboxylate (HPQC) thin films have been studied. Thermogravimetry analysis and differential scanning calorimetry confirmed the thermal stability of HPQC over a wide temperature range. Fourier-transform infrared spectroscopy and x-ray diffraction analysis were carried out on HPQC in powder form and as-deposited thin film. The crystal system and space group type were determined for HPQC in powder form. The AC conductivity and dielectric properties were determined in the frequency range from 0.5 kHz to 5 MHz and temperature range from 296 K to 443 K. The AC electrical conduction of HPQC thin film was found to be governed by the small-polaron tunneling mechanism. The polaron hopping energy (W_H), tunneling distance (R), and density of states (N) near the Fermi level were determined as functions of temperature and frequency. The dielectric properties of HPQC thin film were studied by analysis of Nyquist diagrams, the dissipation factor (tan δ), and real (ε') and imaginary (ε'') parts of the dielectric constant.

Key words: Quinoline, thin film, AC conductivity, small-polaron tunneling mechanism, dielectric properties

INTRODUCTION

Low cost and easy manufacturing are the main reasons for use of organic materials in fabrication of various electronic and photonic devices.[1] Quinoline is an *N*-heterocyclic organic compound in which one of the ring carbon atoms is replaced by nitrogen atom.[1] The donor–acceptor (D–A) nature of the main backbone of quinoline derivative has resulted in great interest for use in the field of organic electronics.[2] Moreover, simple modifications to the donor or acceptor groups can change the physical properties of the quinoline.[2] Quinoline derivatives as organic biologically active compounds are involved in various medical applications.[3] Quinoline derivatives can also be used for synthesis of conjugated molecules and polymers.[4] They are characterized by excellent mechanical properties,[4] thermal stability,[5] high photoluminescence efficiency,[4] nonlinear optical properties,[6] and good film-forming properties,[7] enabling significant applications in highly efficient organic electronics such as optical waveguides,[8] organic light-emitting diodes (OLEDs),[4] dye-sensitized solar cells,[9] and photodiodes.[10]

The physical, e.g., structural, thermal, optical, photovoltaic, electrical, and dielectric, properties of quinoline derivatives depend on the substitution atoms or groups (i.e., electron-withdrawing group, electron-donating group, and metal complex).[7,10–15] In our previous study, the effect of two different donor substitution groups, namely chlorophenyl (Ch-HPQ) and phenoxyphenyl (Ph-HPQ), on the

(Received December 16, 2017; accepted May 18, 2018; published online May 31, 2018)

structural, optical, and dielectric properties of thin films of 4*H*-pyrano[3,2-*c*]quinoline derivatives was investigated.[7,12] Also, the electrical and photoelectrical properties of heterojunction diodes prepared using each compound were investigated based on current–voltage characteristics.[10] Generally, presence of phenoxyphenyl as a more donating substitution group improved the physical properties of the 4*H*-pyrano[3,2-*c*]quinoline derivative thin films. HPQC with the molecular structure shown in Fig. 1 has the Ph-HPQ structure, but the carbonitrile (CN) group is replaced by carboxylate ($CO_2C_2H_5$) group. Literature survey reveals that thermal, structural, AC conductivity, and dielectric studies of HPQC thin film have not been reported to date. Therefore, in the work presented herein, the thermal behavior of this compound was studied to determine the temperature range over which it could be used in different applications. Fourier-transform infrared (FTIR) spectroscopy represents a good tool to study the molecular stability of HPQC against thermal evaporation. Studies of the HPQC structure are very important for better understanding of its transport properties. Also, the alternating-current (AC) conductivity (σ_{AC}) provides deep understanding of the type of conduction mechanism operating in a material. These studies were carried out on HPQC thin films prepared by thermal evaporation technique, sandwiched between two gold electrodes for application in solar cells, photodiodes, and OLEDs in future work.

EXPERIMENTAL PROCEDURES

Fabrication of Samples

Synthesis of HPQC compound in powder form was mentioned in Ref. 16. HPQC thin film was prepared by conventional thermal evaporation technique using a high-vacuum coating unit (model E 306 A, Edwards Co., UK). HPQC was volatilized using a quartz crucible, heated using a molybdenum boat in vacuum of 5×10^{-4} Pa. Film thickness was controlled using a quartz crystal thickness monitor (model, TM-350 Maxtek, Inc., USA). For electrical measurements, HPQC thin film was sandwiched between two gold electrodes, vaporized from a boat-shaped molybdenum filament. The gold was determined to form an ohmic connection with the HPQC thin film.

Thermal Analysis

Thermogravimetry analysis (TGA) and differential scanning calorimetry (DSC) of the HPQC compound in powder form were carried out simultaneously using a Netzsch STA 409 in helium environment in the temperature range of 295 K to 676 K.

Fourier-Transform Infrared Spectroscopy

A PerkinElmer infrared spectrophotometer (model 887) was used to perform FTIR spectroscopy of HPQC in powder and thin film forms. A tablet with thickness of 1 mm and area of 25 mm^2 was formed by mixing 1 mg HPQC powder with 49 mg vacuum-dried IR-grade KBr and compressing using a hydraulic press at pressure of 10 tons cm^{-2} and room temperature.

X-ray Diffraction Analysis

The structure of HPQC in powder form was confirmed by x-ray diffraction (XRD) analysis (Philips X'Pert MPD) using Ni-filtered Cu K_α radiation (λ = 1.5408 Å) with x-ray tube voltage and current of 40 kV and 30 mA, respectively.

AC Electrical Measurements

Electrical measurements were performed by two-point probe technique on HPQC thin film in sandwich structure (Au/HPQC/Au) in air under dark condition. The sample temperature during electrical

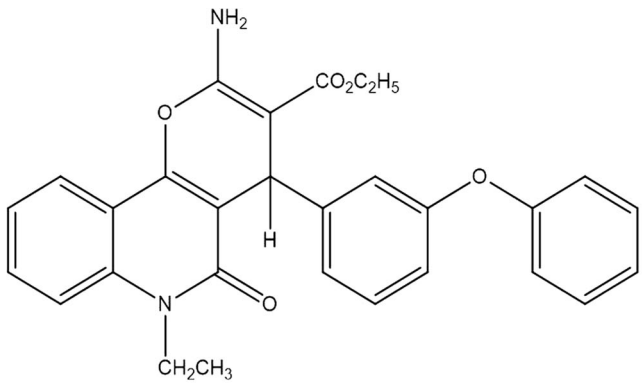

ethyl 2-amino-6-ethyl-5-oxo-4-(3-phenoxyphenyl)-5,6-dihydro-4*H*-pyrano[3,2-*c*]quinoline-3-carboxylate

Fig. 1. Molecular structure of HPQC.

measurements was recorded using a NiCr-NiAl thermocouple.

A programmable automatic *LCR* bridge (Hioki 3532 Hitester) was used to measure the capacitance (C), conductance (G), and dissipation factor (tan δ) of the Au/HPQC/Au sample. Measurements were carried out in the temperature (T) range of 296 K to 443 K and the frequency (f) range of 0.5 kHz to 5 MHz in parallel circuit mode.

RESULTS AND DISCUSSION

Thermal Test

Figure 2a shows the TGA and DTG curves for HPQC compound in powder form. Weight loss was observed at around 260°C due to dissociation of the HPQC molecule backbone.[17] Figure 2b shows the DSC curve of HPQC powder, revealing thermal stability in the temperature range of 25°C to 272°C, in good agreement with the TG analysis. The presence of carboxylate group is responsible for the high thermal stability of HPQC compound.[5] Therefore, all thermal studies on HPQC were performed below 272°C (545 K).

Structural Properties

FTIR Spectroscopy

The FTIR spectra of HPQC compound in powder and thin-film form are shown in Fig. 3a and b, respectively, revealing several absorption bands that were assigned according to Ref. 18 as follows: the three medium peaks at around 3390 cm^{-1}, 3286 cm^{-1}, and 3218 cm^{-1} were attributed to stretching vibrations of N–H in prim-amino (NH_2) groups. The very intense peak at 1685 cm^{-1} is due to stretching vibrations of C=C. The vibration at 1655 cm^{-1} and 1633 cm^{-1} is due to carbonyl group (C=O). The medium peak at 1490 cm^{-1} is attributed to C=C stretching vibrations. The medium peak at 1377 cm^{-1} is due to C–N vibrations. The three peaks at 1284 cm^{-1}, 1255 cm^{-1}, and 120 cm^{-1} are attributed to in-plane C–H bending vibrations of aromatic ring. The four peaks at around 1087 cm^{-1}, 1024 cm^{-1}, 958 cm^{-1}, and 885 cm^{-1} are attributed to alkyl C–C stretching vibration in phenazine ring. The three peaks at around 819 cm^{-1}, 765 cm^{-1}, and 748 cm^{-1} are all attributed to out-of-plane C–H bending vibration in the phenazine ring. The four peaks at around 705 cm^{-1}, 646 cm^{-1}, and 595 cm^{-1} are all attributed to in-plane C–C bending vibration in phenazine ring. The bands were nearly the same for HPQC compound in powder and thin-film form, indicating stable molecular structure of HPQC compound against thermal evaporation.

X-ray Diffraction Analysis

Figure 4a and b show the XRD patterns for HPQC in powder form and as coated thin film, respectively. The many peaks with different intensities in Fig. 4a indicate that HPQC in powder form is polycrystalline. Figure 4b shows amorphous structure for the HPQC thin film. The XRD pattern of HPQC in powder form was indexed using CRYSFIRE software,[19] revealing monoclinic crystal system in space group *P21* with lattice parameters a = 18.66 Å,

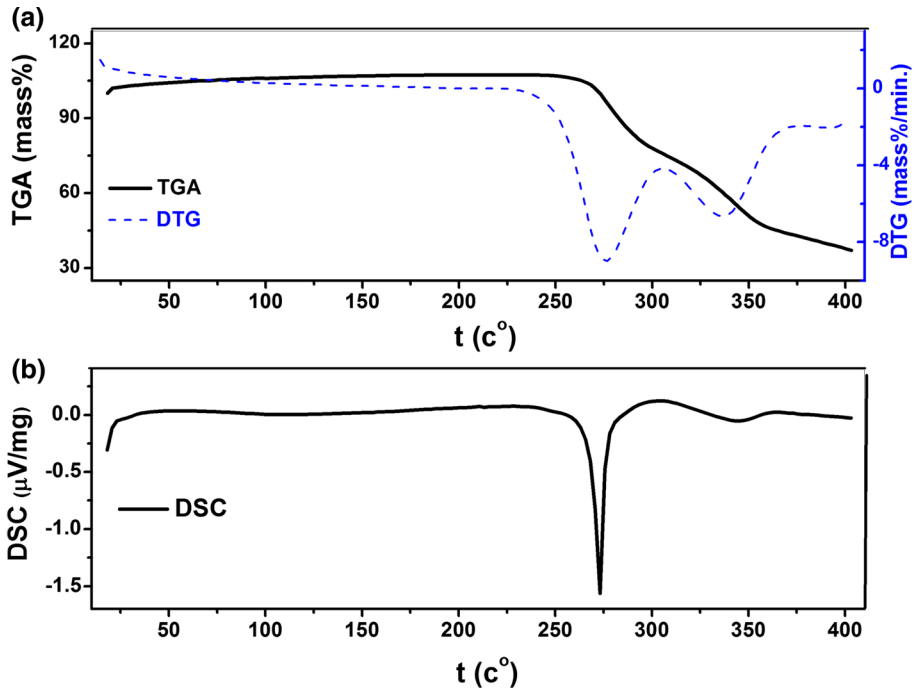

Fig. 2. (a) TGA, DTG, and (b) DSC curves of HPQC compound.

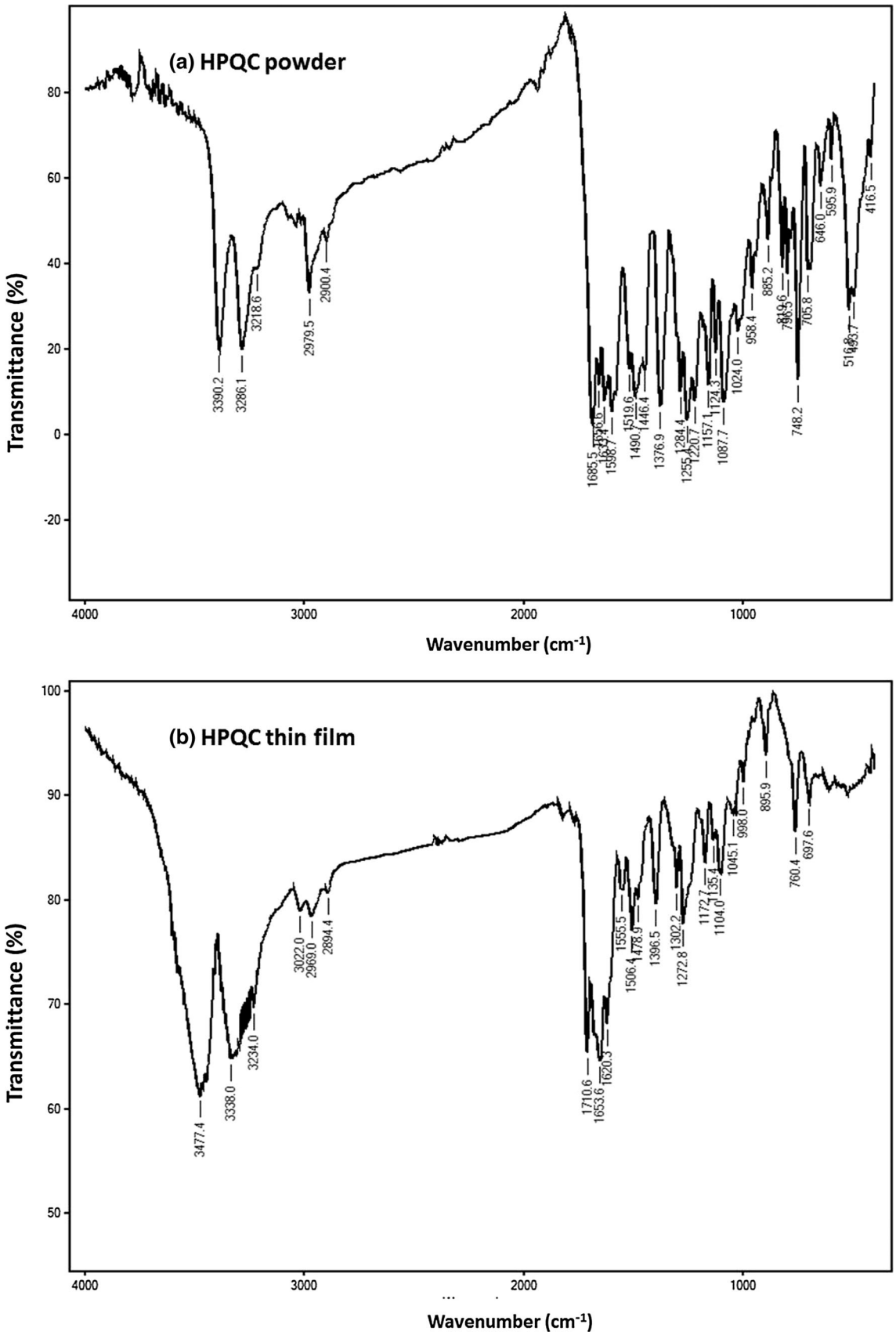

Fig. 3. FTIR spectra for HPQC compound in (a) powder and (b) thin-film form.

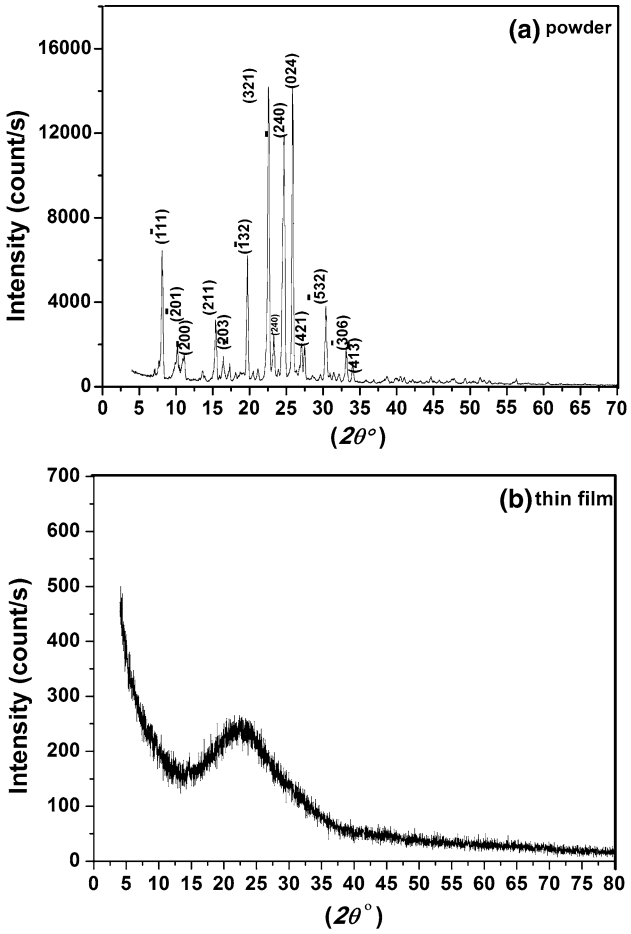

Fig. 4. XRD pattern of HPQC in (a) powder form and (b) as-deposited thin film.

b = 37.32 Å, c = 11.2 Å, $\alpha = 90°$, $\beta = 106.1°$, and $\gamma = 90°$. CHECKCELL software was used to calculate the Miller indices (hkl) for each diffraction peak as shown in Fig. 4a.[20]

AC Conductivity

The measured capacitance (C) and dissipation factor (tan δ) were used to calculate the real (ε') and imaginary parts (ε'') of the dielectric constant using the following relations[21]:

$$\varepsilon' = c\frac{d}{\varepsilon_0 A}, \tag{1}$$

$$\varepsilon'' = \varepsilon' \tan\delta, \tag{2}$$

where $d = 720 \times 10^{-9}$ m and $A = 1 \times 10^{-6}$ m^2 are the thickness and cross-sectional area of the thin film, respectively. ε_0 is the permittivity of free space (8.854×10^{-14} F/cm), and ω is the angular frequency. The AC conductivity σ_{AC} was calculated using the following relation[22]:

$$\sigma_{AC} = \varepsilon_0 \omega \varepsilon''. \tag{3}$$

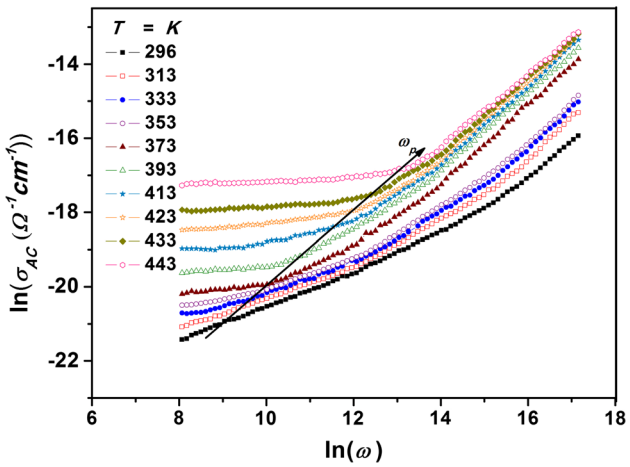

Fig. 5. AC electrical conductivity as function of frequency at various temperatures for Au/HPQC/Au sample.

Figure 5 shows σ_{AC} as a function of frequency for HPQC thin film at various temperatures, revealing a slight increase with frequency at low frequencies but a rapid increment at high frequencies, a behavior observed for different categories of material, including organics,[12,23] polymers,[24] and ceramics.[25] The change in the σ_{AC} behavior occurs at the hopping frequency ω_p, which shifted to higher frequency with increase of temperature. The behavior of σ_{AC} can be fit using the following relation[26]:

$$\sigma_{AC} = \sigma_{DC} + A'\omega^s = \sigma_{DC}\left[1 + (\omega/\omega_p)^s\right], \tag{4}$$

where σ_{DC} is the DC conductivity, A' is a constant, and s is a factor whose magnitude and temperature dependence determine the conduction mechanism in operation. The values of σ_{DC} and ω_p are listed in Table I, increasing with temperature.

Figure 6 shows that the value of s in the high-frequency region increased with temperature. Many theories have been applied to explain the AC conductivity of disordered materials.[27,28] The above data trend for s is indicative of the small-polaron tunneling mechanism (SPTM), as found for many quinoline derivative complexes[14,29] and other organic compounds.[30] For the SPTM, the AC conductivity σ_{AC} is given by the following equation[28]:

$$\sigma_{AC} = \frac{(\pi e)^2}{12} K_B T \alpha^{-1} \omega N^2 R^4, \tag{5}$$

where α^{-1} is the spatial extension of the polaron (α^{-1} = 1 Å^{-1} [31]), N is the density of states near the Fermi level, and R is the tunneling distance, given by the following relation[28]:

$$R = \frac{1}{2\alpha}\left[\ln\left(1/\omega\tau_0\right) - \left(W_H/K_B T\right)\right], \tag{6}$$

where τ_0 is the characteristic relaxation time, on the order of an atomic vibrational period $\sim 10^{-13}$ s[32] and W_H is the polaron hopping energy. The

Table I. Calculated values of σ_{DC} and ω_p at different temperatures for HPQC thin film

T (K)	$\sigma_{DC} \times 10^{-10}$ (Ω^{-1} cm^{-1})	ω_p (kHz)
296	0.6	7.04
313	0.84	8.26
333	1.1	9.51
353	1.6	10.4
373	5.7	15.3
393	15	22.9
413	16.8	28
423	30.7	156
433	79.5	252.7
443	193	488.9

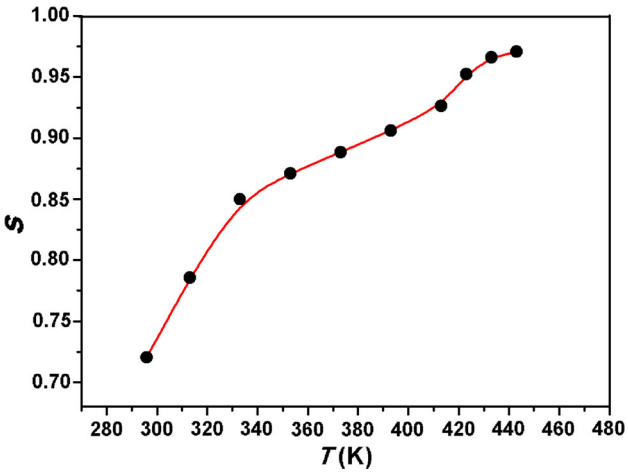

Fig. 6. Variation of frequency exponent s of Au/HPQC/Au sample with temperature.

frequency exponent s for SPTM can be evaluated using the following relation[28]:

$$s = 1 - \frac{4}{\ln\left(1/\omega\tau_0\right) - \left(W_H/K_B T\right)}. \quad (7)$$

The value of W_H can be calculated by fitting of Eq. 7, yielding a value of 0.5 eV. The dependence of the tunneling distance R on frequency for the HPQC thin film at various temperatures is shown in Fig. 7. The tunneling distance decreased with increase of both frequency and temperature. The magnitude of R is on the order of 10^{-10} cm, comparable to values for organic compounds from the same family as well as other quinoline derivatives.[12,15,30] Figure 8 shows the dependence of N on frequency and temperature for the HPQC thin film. The value of N increased exponentially with increasing frequency and linearly with increasing temperature. The magnitude of N is on the order of 10^{27} eV cm^{-3}, comparable to values for other quinoline derivatives.[12,15,30] It is obvious that σ_{AC} increases with

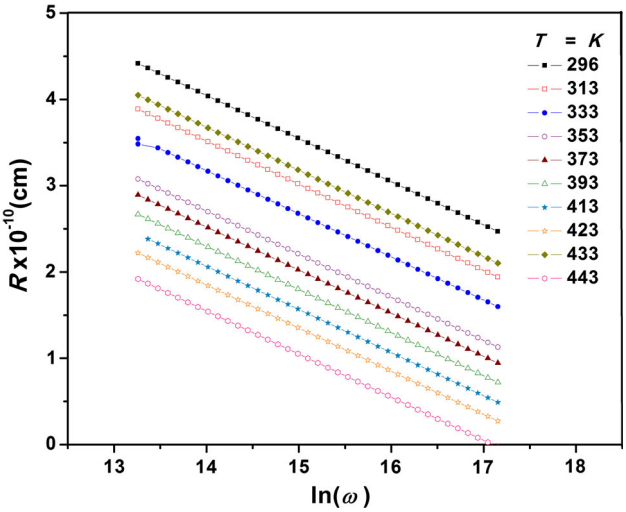

Fig. 7. Frequency dependence of tunneling distance R for Au/HPQC/Au sample at various temperatures.

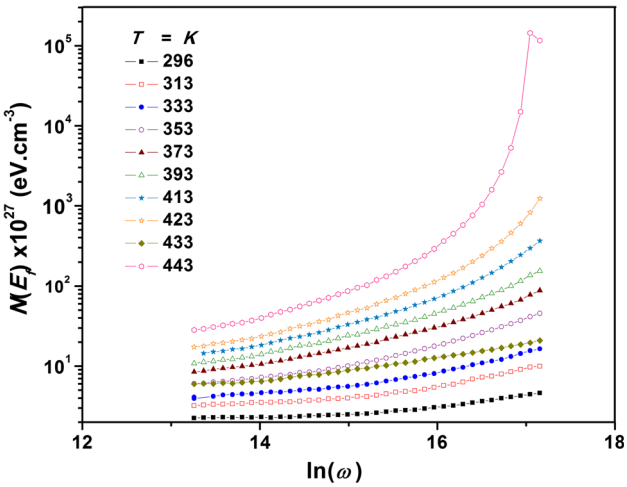

Fig. 8. Frequency dependence of density of states N for Au/HPQC/Au sample at various temperature.

frequency due to the increase of N and decrease of R.

The temperature dependence of σ_{AC} was studied at different frequencies. Figure 9 shows plots of ln σ_{AC} against 1000/T for HPQC thin film. It is clear that the electrical conductivity increased linearly with increasing absolute temperature. The plots exhibit two separate regions with different slopes, suggesting that the electrical conductivity is a thermally activated process from different localized states in the gap or its tails.[33] The activation energy for conduction ΔE was calculated at different frequencies from the slopes of lines in Fig. 9 using the Arrhenius law[34]:

$$\sigma = \sigma_0 \exp\left(\Delta E/K_B T\right), \quad (8)$$

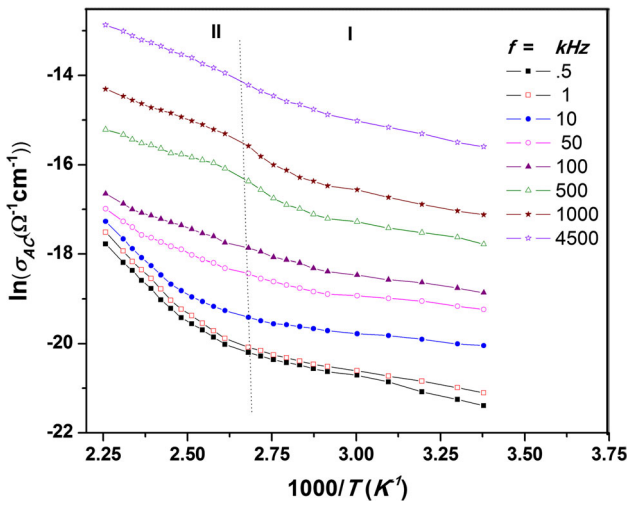

Fig. 9. AC conductivity as function of temperature at different frequencies for Au/HPQC/Au sample.

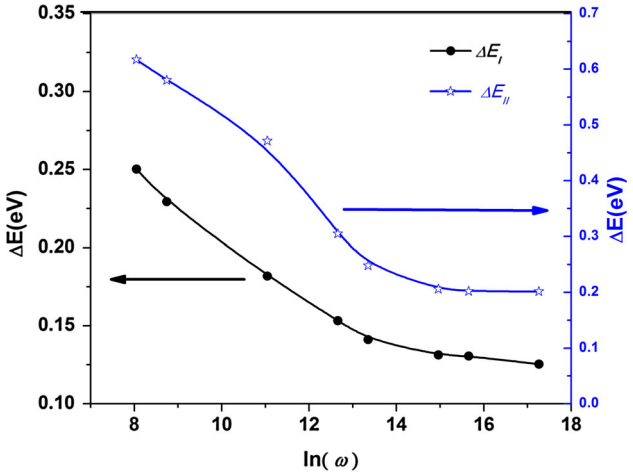

Fig. 10. Variation of activation energy with frequency for Au/HPQC/Au sample.

where σ_0 is the preexponential factor and ΔE is the AC activation energy for conduction. The obtained values of ΔE_{I} at low temperatures and ΔE_{II} at relatively high temperatures were found to decrease exponentially with increasing frequency, as shown in Fig. 10. The decrease of ΔE with frequency can be attributed to electronic jumps between localized states as the frequency of the applied field is increased.[35]

Impedance Studies

The dielectric properties of HPQC were investigated using the complex impedance (Z^*), complex permittivity (ε^*), and dissipation factor ($\tan\delta$) in the frequency range of 0.5 kHz to 5 MHz at different temperatures. The real (Z') and imaginary parts (Z'') parts of Z^* can be estimating from the

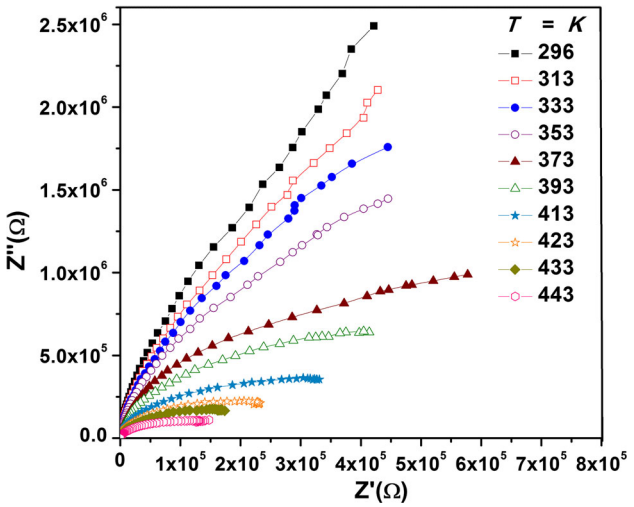

Fig. 11. Nyquist plots for Au/HPQC/Au sample at different temperatures.

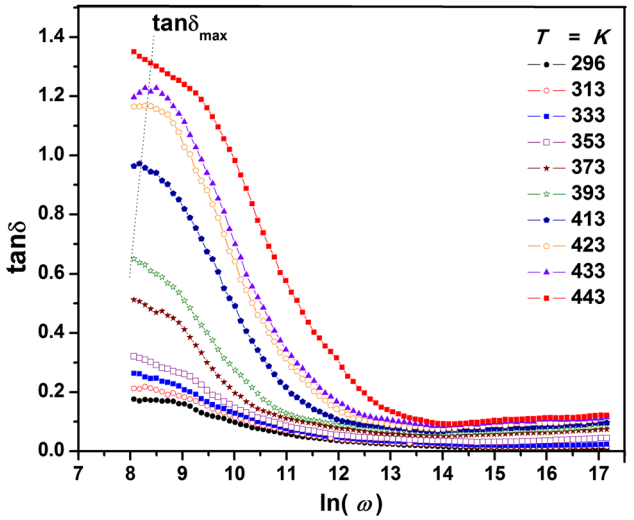

Fig. 12. Frequency dependence of dissipation factor ($\tan\delta$) for Au/HPQC/Au sample at different temperatures.

measured parallel G and C using the following relations[36]:

$$Z' = \frac{G}{G^2 + \omega^2 c^2}, \tag{9}$$

$$Z'' = \frac{c\omega}{G^2 + \omega^2 c^2}. \tag{10}$$

Figure 11 shows the Nyquist plots for HPQC thin film at different temperatures. At the lower temperatures, the Nyquist plots are nearly straight lines. The linear slope decreased with increasing temperature, and the lines transformed to arcs with increasing temperature. Such deviations from ideal RC behavior may be due to the existence of a constant-phase element (CPE).[37–39]

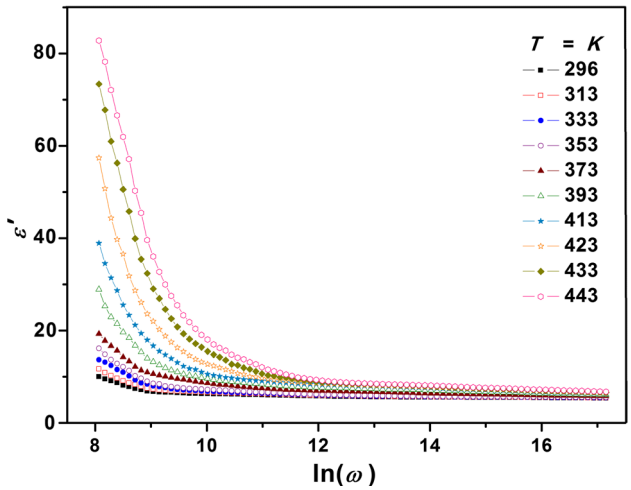

Fig. 13. Frequency dependence of ε' for Au/HPQC/Au sample at different temperatures.

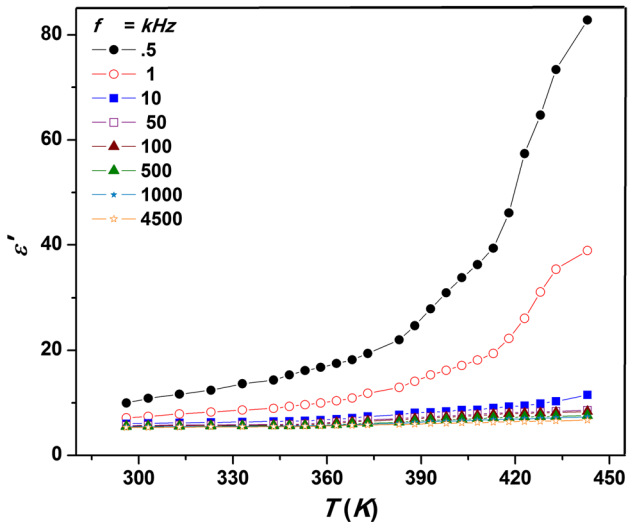

Fig. 14. Temperature dependence of ε' for Au/HPQC/Au sample at different frequencies.

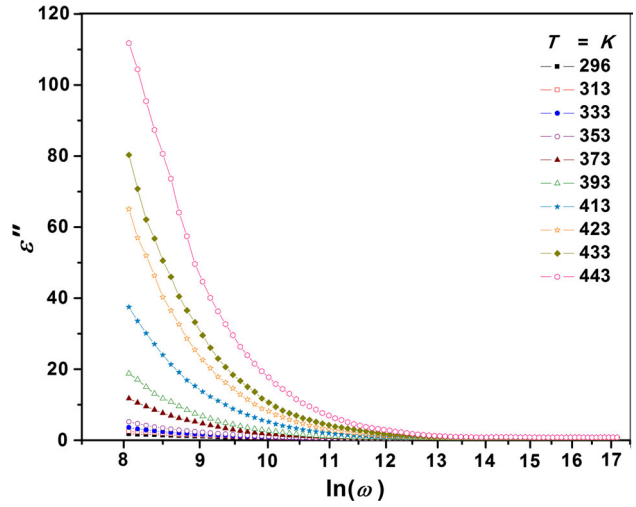

Fig. 15. Frequency dependence of ε'' for Au/HPQC/Au sample at different temperatures.

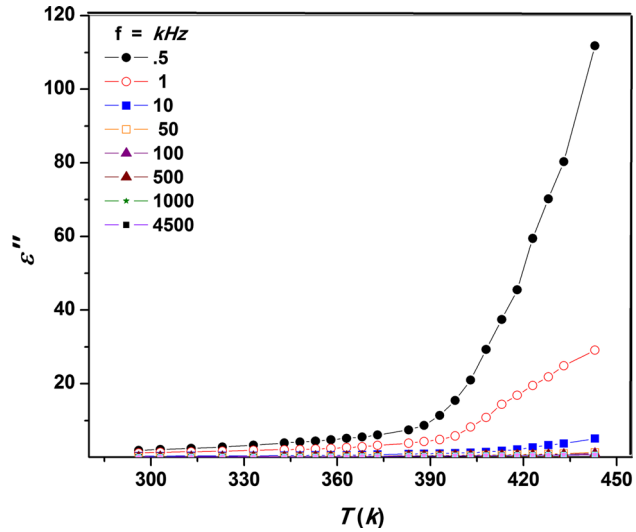

Fig. 16. Temperature dependence of ε'' for Au/HPQC/Au sample at different frequencies.

Figure 12 shows that tan δ increased slowly with rising temperature but decreased with increasing frequency. At low temperatures, no peaks were found as a function of frequency. At higher temperatures, one peak was observed in the low-frequency region, shifting to higher frequency with increasing temperature. This behavior may be due to loss dominated by thermally activated carrier hopping across a barrier at higher temperatures.[40]

Figure 13 shows that ε' decreased with increasing frequency at constant temperature. No peaks were found as a function of frequency, which may be considered to indicate that a lattice polarization-type phenomenon with dipole formation did not occur.[41] Figure 14 shows ε' as a function of temperature at constant frequency. Note that ε' showed strong temperature dependence at low frequencies but was nearly constant at high frequencies. The increase of ε' with temperature can be attributed to polarization connected with thermal motion of electrons.[42]

Figure 15 shows that ε'' decreased with increasing frequency at constant temperature. Dielectric loss originates from conduction, dipole, and vibrational losses.[1] Also, it increased slowly at lower temperatures then sharply with further temperature increment at constant frequency, as shown in Fig. 16. The increase of ε'' with temperature can be attributed to the fact that dipoles in polar materials cannot orient themselves at low temperatures.

When this becomes possible, the orientation polarization increases, thereby increasing ε'.[43]

CONCLUSIONS

DSC and TG confirmed that HPQC is thermally stable in a wide temperature range from 295 K to 545 K. FTIR spectroscopy indicated stability of the molecular structure of HPQC compound against thermal evaporation. XRD analysis of HPQC in powder form revealed monoclinic crystal system in space group *P21* with lattice parameters $a = 18.66$ Å, $b = 37.32$ Å, $c = 11.2$ Å, $\alpha = 90°$, $\beta = 106.1°$, and $\gamma = 90°$. As-deposited thin film showed amorphous structure. The AC electrical conduction in HPQC thin film is governed by the small-polaron tunneling mechanism (SPTM). W_H was calculated to be 0.5 eV, the magnitude of R was on the order of 10^{-10} cm, the values of N increased exponentially with increasing frequency and linearly with temperature, being on the order of 10^{27} eV cm^{-3}. The temperature dependence of the AC conductivity was studied at different frequencies. The obtained values of ΔE_I at low temperatures and ΔE_{II} at relatively high temperatures were found to decrease exponentially with increasing frequency. Impedance data are presented as Nyquist diagrams for different temperatures. The dielectric properties of HPQC in thin-film form, including tan δ, ε', and ε'', increased slowly with temperature but decreased with increasing frequency.

ACKNOWLEDGEMENTS

The author thanks Professor Dr. F. M. El-Taweel, Department of Chemistry, Faculty of Science, Damietta University, for synthesis of HPQC compound.

REFERENCES

1. M.M. El-Nahass and H.A.M. Ali, *Solid State Commun.* 152, 1084 (2012).
2. E.E. Havinga, W. ten Hoeve, and H. Wynberg, *Polym. Bull.* 29, 119 (1992).
3. A. Zablotskaya, I. Segal, A. Geronikaki, I. Shestakova, V. Nikolajeva, and G. Makarenkova, *Pharmacol. Rep.* 69, 575 (2017).
4. G.C. dos Santos, R.O. Servilha, E.F. de Oliveira, F.C. Lavarda, V.F. Ximenes, and L.C. da Silva-Filho, *J. Fluoresc.* 27, 1709 (2017).
5. M.H. Keshavarz, A. Mousaviazar, and M. Hayaty, *J. Therm. Anal. Calorim.* 3, 1659 (2017).
6. S. Arroudj, A. Aamoum, L. Messaadia, A. Bouraiou, S. Bouacida, K. Bouchouit, and B. Sahraoui, *Phys. B Condens. Matter* 516, 1 (2017).
7. H.M. Zeyada, M.M. El-Nahass, and M.M. El-Shabaan, *Philos. Mag.* 96, 1150 (2016).
8. N. Wickremasinghe, J. Thompson, X. Wang, H. Schmitzer, and H.P. Wagner, *J. Appl. Phys.* 117, 213102 (2015).
9. R. Fan, X. Wang, Y. Dong, T. Su, J. Huang, X. Du, P. Wang, and Y. Yang, *Cryst. Growth Des.* (2017). https://doi.org/10.1021/acs.cgd.7b00891.
10. H.M. Zeyada, M.M. El-Nahass, and M.M. El-Shabaan, *Synth. Met.* 220, 102 (2016).
11. A.M. Mansour, F.M.A. El-Taweel, R.A.N. Abu El-Enein, and E.M. El-Menyawy, *J. Electron. Mater.* 12, 6957 (2017).
12. H.M. Zeyada, F.M. El-Taweel, M.M. El-Nahass, and M.M. El-Shabaan, *Chin. Phys. B* 25, 077701 (2016).
13. N.A. El-Ghamaz, E.M. El-Menyawy, M.A. Diab, A.A. El-Bindary, A.Z. El-Sonbati, and S.G. Nozha, *Solid State Sci.* 30, 44 (2014).
14. N.A. El-Ghamaz, M.A. Diab, A.A. El-Bindary, A.Z. El-Sonbati, and S.G. Nozha, *Spectrochim. Acta. A. Mol. Biomol Spectrosc.* 143, 200 (2015).
15. H.M. Zeyada, N.A. El-Ghamaz, and E.A. Gaml, *Phys. B Condens. Matter* 519, 76 (2017).
16. F.M.A. El-Taweel, A.A. Elagamey, and M.H.M. Khalil, *Am. Chem. Sci. J.* 3, 532 (2013).
17. A. Mohamed Saat and M.R. Johan, *Sci. World J.* 2014, 1 (2014).
18. Z. Yan, S. Guang, H. Xu, X. Su, X. Ji, and X. Liu, *RSC Adv.* 3, 8021 (2013).
19. R. Shirely, The CRYSFIRE system for automatic powder indexing: User's manual, Guildford, Surrey GU2 7NL England the Lattice Press, 2002.
20. J. Laugier and B. Bochu, LMGP-suite site of programs for the interpretation of X-ray experiments, BP 46, 38042, ENSP/Laboratoire des Materiaux et du Genie Physique, Saint Martin d'Heres, 2000.
21. A. Ghosh, *Phys. Rev. B* 42, 5665 (1990).
22. S.R. Elliott, *Adv. Phys.* 36, 135 (1987).
23. E.M. El-Menyawy, I.T. Zedan, and A.M. Mansour, *J. Electron. Mater.* 46, 4353 (2017).
24. T. Winie and A.K. Arof, *Ionics* 10, 193 (2004).
25. K.S. Rao, K.C.V. Rajulu, and B. Tilak, *Int. J. Mod. Phys. B* 25, 2931 (2011).
26. D. Almond, G. Duncan, and A. West, *Solid State Ion.* 8, 159 (1983).
27. A.R. Long, *Adv. Phys.* 31, 553 (1982).
28. S.R. Elliott, *Adv. Phys.* 36, 135 (1987).
29. N.A. El-Ghamaz, A.Z. El-Sonbati, M.A. Diab, A.A. El-Bindary, and S.M. Morgan, *Mater. Res. Bull.* 65, 293 (2015).
30. A. Kahouli, A. Sylvestre, F. Jomni, B. Yangui, and J. Legrand, *J. Phys. Chem. A* 116, 1051 (2012).
31. B.N. Pal and D. Chakravorty, *Sens. Actuators B Chem.* 114, 1043 (2006).
32. V.K. Bhatnagar and K.L. Bhatia, *J. Non-Cryst. Solids* 119, 214 (1990).
33. N.F. Mott and E.A. Davis, *Electronic processes in non-crystalline materials*, 2nd ed. (Oxford: Clarendon, 2012).
34. T. Badapanda, V. Senthil, S.K. Rout, L.S. Cavalcante, A.Z. Simoes, T.P. Sinha, S. Panigrahi, M.M. de Jesus, E. Longo, and J.A. Varela, *Curr. Appl. Phys.* 11, 1282 (2011).
35. M. Okutan, E. Basaran, H.I. Bakan, and F. Yakuphanoglu, *Phys. B Condens. Matter* 364, 300 (2005).
36. C. Mariappan and G. Govindaraj, *Solid State Ion.* 176, 1311 (2005).
37. P.S. Germain, W.G. Pell, and B.E. Conway, *Electrochim. Acta* 49, 1775 (2004).
38. E. Barsoukov and J.R. Macdonald, *Impedance spectroscopy theory, experiment, and applications* (Hoboken: Wiley-Interscience, 2005).
39. M.M. El-Shabaan, *J. Electron. Mater.* (2018). https://doi.org/10.1007/s11664-018-6098-8.
40. S. Tewari, A. Bhattacharjee, and P.P. Sahay, *J. Mater. Sci.* 44, 534 (2009).
41. M.A.L. Nobre and S. Lanfredi, *Mater. Lett.* 47, 362 (2001).
42. M.M. El-Nahass, H.A.M. Ali, and E.F.M. El-Zaidia, *Phys. B Condens. Matter* 431, 54 (2013).
43. M.A.M. Seyam, *Appl. Surf. Sci.* 181, 128 (2001).